ELSEVIER

Contents lists available at ScienceDirect

Journal of Manufacturing Processes

journal homepage: www.elsevier.com/locate/manpro





Machine learning model for understanding laser superhydrophobic surface functionalization

Wuji Huang ^a, Avik Samanta ^a, Yong Chen ^b, Stephen Baek ^b, Scott K. Shaw ^c, Hongtao Ding ^a, ^a

- ^a Department of Mechanical Engineering, University of Iowa, Iowa City, IA 52242, USA
- ^b Department of Industrial and Systems Engineering, University of Iowa, Iowa City, IA 52242, USA
- ^c Department of Chemistry, University of Iowa, Iowa City, IA 52242, USA

ARTICLE INFO

Keywords: Machine learning Superhydrophobic surface Surface functionalization Laser surface processing Surface chemistry

ABSTRACT

A general machine learning (ML) framework of surface wetting is proposed by considering a broad range of factors, including solid surface topography, solid surface chemistry, liquid properties, and environmental conditions. In particular, an XGBoost-based ML model is demonstrated for learning the surface wetting behaviors processed by a laser-based surface functionalization process, namely nanosecond laser-based high-throughput surface nanostructuring (nHSN). This is the first known attempt to apply machine learning to surface wetting by considering both surface topography and surface chemistry properties. Novel microscale and nanoscale topography parameters viz., roughness, fractal, entropy, feature periodicity are defined with suitable computer algorithms to comprehensively describe the surface topography. A novel set of surface chemistry parameters such as polarity, volume, and amount of functional groups are also used as the machine learning model input. Upon analyzing the importance of each parameter for the nHSN process, surface chemistry shows the greatest importance in determination of surface wettability, while surface morphology also plays a part in influencing the wettability.

1. Introduction

Wettability of a solid surface is defined by its ability to maintain contact with a fluid and is often characterized using contact angle (θ) at the meeting point of liquid-gas and solid-liquid interfaces. Depending on the wetting condition, solid-liquid interface can have a critical impact in ubiquitous engineering applications, and therefore has aroused intense interest. Surface wetting is governed by the balance between the intermolecular interactions at the solid-liquid interface [1] and is influenced by many factors, including liquid properties, solid surface properties, and environmental conditions. The solid surface wettability can be physiochemically engineered by modifying its surface morphology [2,3] and/or surface chemistry [4,5].

Extensive material research has shown that surface topography, i.e., surface roughness and surface texture, of a solid material can be modified to obtain desirable wetting properties regarding a liquid. In the presence of increasing roughness, water contact angle increases for hydrophobic materials and decreases for hydrophilic materials [6–8]. For instance, Busscher et al. [7] measured contact angles for five different liquids on twelve commercial polymers after various surface

roughness procedures and reported that, if the contact angle was above 86° , the increase of surface roughness led to increasing contact angle; whereas if the contact angle was below 60° , the surface roughening tended to decrease the contact angle. Veeramasuneni et al. [8] reported similar results by investigating the influence of surface roughness on the wetting behavior of ion-plated poly(tetrafluoroethylene) (PTFE) coatings. They found that the nanoscale surface asperities tended to increase the water contact angle in superhydrophobic range (150° $\sim 160^\circ$). AlRatrout et al. [9] studied the impact of surface roughness on wettability in the porous region of limestone, and showed that the range of distribution of oil contact angle increased with the degree of roughness. Belaud et al. [10] investigated the impact of roughness on static contact angle measured on polypropylene textured surfaces and proposed a model describing the correlation between the contact angle and surface roughness parameters.

Various surface texturing techniques, particularly laser materials processing, have been applied to create fine textures or patterns on materials in order to achieve desired wetting behavior. Ahuir-Torres et al. [11] generated three types of texture patterns on aluminum alloy using an infrared picosecond laser. It was found that the un-

E-mail address: hongtao-ding@uiowa.edu (H. Ding).

^{*} Corresponding author.

textured surface and the surface with dimples showed hydrophilic behavior, while the surface with crossed grooves and the concentric rings exhibited a hydrophobic character. Jiao et al. [12] generated a dimple pattern and groove pattern on a Zr-based bulk metallic glass. They found that the hydrophilicity of the original surface was enhanced by the groove pattern and weakened by the dimple pattern. Granados et al. [13] demonstrated that the formation of laser-induced periodic surface structures (LIPSS) in boron-doped diamond by irradiation with femtosecond laser leads to hydrophilic behavior. Superhydrophilicity can also be achieved on stainless steel by LIPSS formation, and θ increases with the laser scanning speed [14]. Batal et al. [15] found that LIPSS on polished CoCrMo alloy increased θ value from 46.0° to 54.7°, and the contact angle growth was also influenced by laser processing parameters, including beam incident angle and focal offset distance. Orazi et al. [16] reported that LIPSS turned surface behavior from hydrophilicity to hydrophobicity for stainless steel, copper, and aluminum

Numerous research efforts have been devoted to modifying the surface chemistry to achieve desirable wetting behavior. Surface functionalization methods introduce hydrophobic or hydrophilic chemical functional groups to a solid surface in order to achieve desired hydrophobicity or hydrophilicity, respectively. Liang et al. [17] reported that the wettability of candle soot varied from superhydrophobicity to hydrophilicity due to different chemical compositions, yet their research did not assess any quantitative relationship between the contact angle and the chemical composition. Pan et al. [18] investigated the rapid wettability switching of silane-modified TiO2 particles. Upon ultraviolet illumination, the TiO2 particles switched from a superhydrophobic state $(\theta \sim 165^{\circ})$ to a superhydrophilic state $(\theta \sim 0^{\circ})$ due to UV-induced oxidation. Psarski et al. [19] modified SU-8 surfaces with a homologous series of fluoroalkyl silanes to investigate the influence of surface chemistry on surface wettability. They found that the higher the surface density of low surface free energy groups (-CF2- and -CF3) the higher the advancing contact angle. Surface chemistry modification was also combined with surface morphology to alter wettability. Zhang et al. [20] made a topography/chemical composition gradient polystyrene (PS) surface and established the relationship between wettability and surface roughness and chemical composition. In this study, a series of PS with various degrees of sulfonation was formed on the surface. It was found that θ increases with roughness as well as sulfonation degree. Zhang et al. [21] prepared a smart surface on pillar-structured shape memory polymer, which can switch between superhydrophobicity to superhydrophilicity by tuning surface microstructure and surface chemistry.

Superhydrophobic surfaces have received a growing interest among researchers across the world, and the number of technical publications on superhydrophobic surfaces continues to increase, demonstrating expanding impacts. As shown in Fig. 1, thousands of technical papers have been published in the last decade. Although a myriad of work has been done to study the effect of different factors affecting wetting

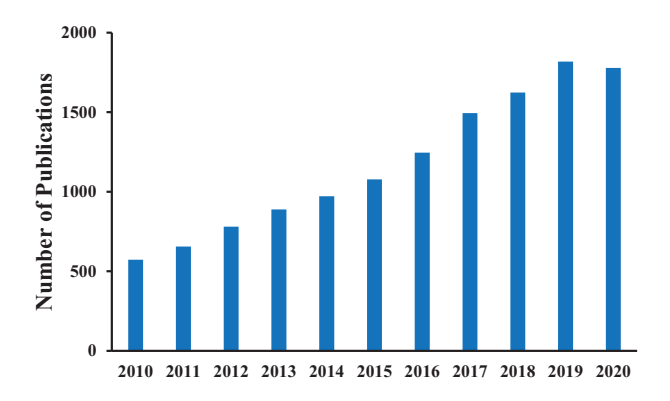


Fig. 1. The number of publications taken from Web of Science on the topic of superhydrophobic surface between the years 2010 and 2020.

property of surface, the state-of-the-art research efforts are primarily experimental with a focus on materials innovation. Given the complex coupling effect among all the factors and their huge parameter space contributing to surface wetting, the published research in literature often time considered only a narrow set of factors or conditions. On the other hand, classic analytical models have been employed in the past two centuries to explain the wetting behavior of a solid surface, including Young's model, Wenzel's model [22], and Cassie-Baxter model [23]. However, these deterministic analytical models theorize the solid surface to ideal conditions and consider a limited number of factors such as liquid surface tension and solid surface roughness. Recent computational methods, including molecular dynamics [24] and density functional theory [25] have been applied to study wettability; nonetheless, only ideal wetting conditions were considered. It is therefore critical to develop a comprehensive, predictive relationship among surface engineering/manufacturing processes, surface phytochemical attributes and surface wettability.

A general machine learning (ML) framework is firstly proposed in this study for surface wetting prediction considering a broad range of factors affecting surface wetting behavior. As discussed earlier, data from the published research works are usually fragmented and only cover a narrow set of factors. Therefore, a novel laser-based nanostructuring process was designed in our own case study to acquire various surface morphology and chemistry data as the input for ML. A series of parameters were developed to describe the surface topography as well as surface chemistry and were used as input to feed an XGBoost ML model to predict water contact angle (θ_w). Although the ML model for this case study uses a limited dataset, the inner relationship between the parameters and the water contact angle is complex and nonlinear. Hence it is necessary to apply an ML method to deal with complex nonparametric patterns in the data. This study demonstrated the effectiveness of XGBoost in handling such complex nonlinear data. Upon feature importance analysis, the importance of surface chemistry on wetting was established. To the authors' best knowledge, this is the first effort to use machine learning to predict wettability based on surface morphology and chemistry. Although the method proposed in this research is applied for laser surface processing, it is equally applicable for the wettability prediction of other methods.

2. Machine learning framework for surface wetting

In this work, a comprehensive ML framework is introduced for predicting the surface wettability of a solid material based on the vast knowledge gained from literature. As can be seen in Fig. 2, the input of the proposed ML model includes a broad range of factors affecting surface wetting, i.e., solid surface topography, solid surface chemistry, liquid properties, and environmental conditions. The outputs of the ML model are surface wettability properties such as contact angle and solidliquid interaction strength. A key challenge for the development of such an ML model is that the input data have various forms and structures: qualitative and quantitative data, continuous and discrete data, field raw data, and processed data. The proposed ML model is expandable to adapt to different types and sizes of a dataset. When one performs experiments and collects new data related to surface wettability, the new data can be easily incorporated without changing the algorithm. The adaptability makes the machine learning method quite promising to determine the process-surface-wettability relationship. The objective of the proposed ML model is to establish a quantifiable, predictive relationship between wettability and myriad factors that can influence wetting. The developed ML model will greatly aid in designing and optimizing material processes to achieve a specific desired wettability. By analyzing the relationship between the process parameters and wettability, the machine learning model is capable of providing guidance for the design of processes to achieve specific surface properties. Furthermore, the ML model can even be expanded to make predictions of other surface properties, e.g., surface adsorption, absorption/

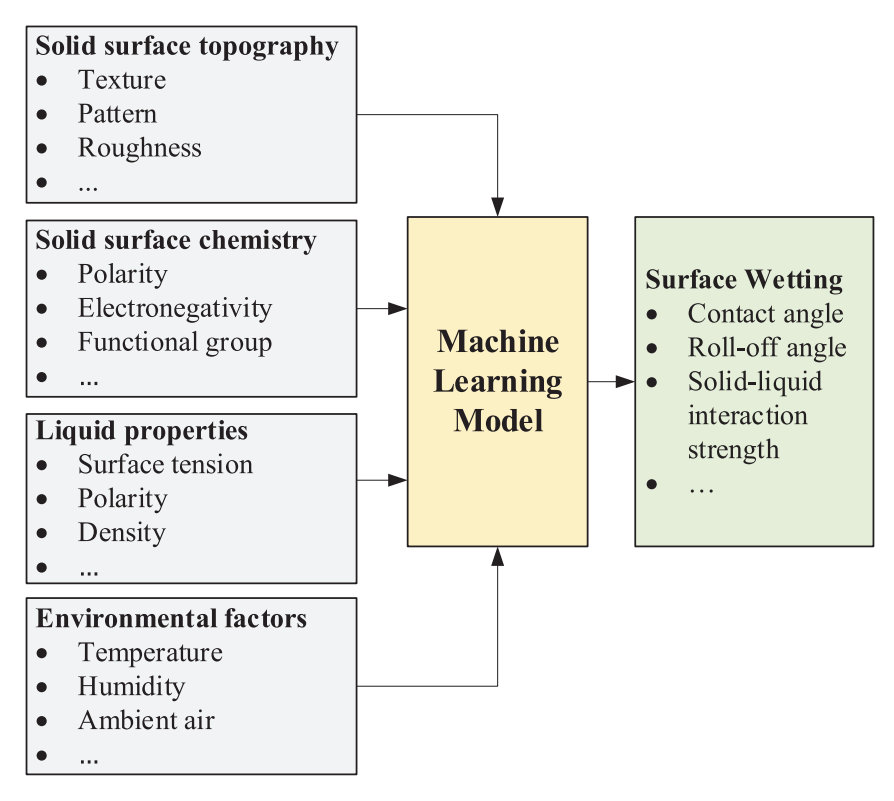


Fig. 2. General framework of machine learning of surface wetting behaviors.

reflection, and corrosion.

Data-driven ML methods are becoming ubiquitous due to the recent advances in computational power and techniques. They have been used to explore materials and structures and to extract meaningful information and patterns from existing data [26]. Among all different types of machine learning algorithms, regression is one of the most important and widely used machine learning tools to make predictions from data by learning the relationship between numeric features of the data and the continuous-valued response. In this research, a continuous value, the wettability of metal surfaces (contact angle), is proposed to be predicted through a regression model. There are several well-developed machine learning models to deal with regression models, including Artificial Neural Networks (ANNs), Support Vector Machines (SVMs), and Regression Trees [27]. ANN models are inspired by biological neural networks, which are used to estimate the relationship between the inputs and outputs [28], and are effective when dealing with complex, non-linear problems. SVM models are based on the concept of maximizing the minimum distance from the hyperplane to the nearest sample point [29]. They can be used both for classification and regression problems. The original SVM for regression (SVR) was developed by Vapnik et al. [30] and is capable of dealing with non-linear problems. Another machine learning model used to deal with complex and nonlinear data is Random Forest (RF), developed by Breiman [31], which is an ensemble learning method that combines a bunch of Regression Trees to construct a forest. Each tree produces a response, while the forest averages the predictions from all of the trees contained in the forest. In addition, extreme gradient boosting (XGBoost) is a robust machine learning algorithm proposed by Chen et al. [32] for both regression and classification problems. It has the merit of high effectiveness and accuracy over several other machine learning algorithms such as SVMs and regression trees [33,34]. All of the machine learning models above make it possible to predict the contact angle by learning from the surface structure data and the surface chemistry data.

As can be seen in Fig. 2, the solid surface topography data serves as an important input data category for the proposed ML model. The

topography data are usually obtained by surface microscopy techniques, including surface profilometer, digital camera, optical microscopy (OM), white-light interferometry (WLI), scanning electron microscope (SEM), atomic force microscope (AFM), and confocal microscopy (CM). Surface roughness is often a good predictor of the performance of a solid surface and is quantified by the deviations in the direction of the normal vector of a real surface from its ideal form. Quick measurements can be obtained using a surface profilometer and WLI. The images from OM mostly provide low magnification surface features, whereas the images obtained from SEM can be processed to extract relevant information regarding the microscale or nanoscale features. The AFM is a very high-resolution microscopy with a typical resolution on the order of fractions of a nanometer, more than 1000 times better than the optical diffraction limit. CM, WLI, and surface profilometer can all provide the spatial distribution of roughness across the surface.

Surface chemistry data can be obtained from various surface chemical analysis techniques. Surface functional groups are commonly detected through X-ray photoelectron spectroscopy (XPS). Energy dispersive spectroscopy (EDS) analysis can be used to determine the elements presented on the surface. Chemical identity, bonding, and environment can be verified by the Fourier transfer infrared (FTIR) spectra. The characteristic peaks can be used for analysis since they are indicators of specific chemical bonds or chemical elements. For example, both the peak position and peak height of the XPS spectrum can be used as the input of a machine learning model as they represent the type of chemical element and the concentration of that element in the sample, respectively. Some fundamental physical or chemical properties of the surface chemicals, such as the oxidation state of the molecules, can also be used as the input since the physical properties also play a significant role in the determination of the interaction between the surface and the liquid.

The physical and chemical properties of liquids are also important input, including surface tension, viscosity, Hamaker constants, interaction potentials, etc. Environmental parameters, including temperature, pressure, and humidity, also impact the surface wettability. They can be

measured by thermometer, hygrometer, barometer, etc. Thus, the environmental factors can also be incorporated into the input data to teach the machine learning model to predict wettability in any environmental setting.

Wettability of a specific surface can be defined using several variables as the ML model output. The most commonly used variable is the equilibrium contact angle of a static droplet sitting on a solid surface. There are other variables to comprehensively define wettability. For non-equilibrium interaction, the dynamic contact angle is usually measured. For a hydrophobic surface, other variables are used along with static contact angle, including roll-off angle ($\theta_{Roll-off}$), advancing contact angle (θ_{Adv}), receding contact angle (θ_{Rec}), and contact angle hysteresis (θ_{Hvs}). $\theta_{Roll-off}$ is the angle of inclination of a solid surface at which a droplet starts to roll off. θ_{Adv} and θ_{Rec} are the contact angles when a water droplet approaches and recedes from a surface, respectively. θ_{Hvs} is the difference between θ_{Adv} and θ_{Rec} in a measurement cycle. All these angles can be measured by the well-developed contact angle goniometers. Since these variables are numerical values, they can be easily used as the output of a machine learning regression algorithm. By applying machine learning methods, a lot of bench work can be saved since it points out what kind of surface to create for a set of material properties.

3. ML model for nHSN superhydrophobic surface processing

In this section, a case study of the proposed ML framework was presented for the prediction of surface wettability of metal alloys to water under lab-controlled environments. As shown in Fig. 3, the field data of the study was generated, collected, extracted, and processed by the authors using a novel nanosecond laser-based high-throughput surface nanostructuring (nHSN) process [35-38] that can simultaneously create random nanostructures and attain desirable surface chemistry over large-area metal alloy surfaces. By altering the processing conditions, the nHSN treated surfaces manifested different wetting behaviors ranging from superhydrophobicity to superhydrophilicity. The XGBoost model was used to learn the relationship between the surface topography, surface chemistry, and the wettability of these nHSN treated surfaces. To the authors' best knowledge, this study constitutes the first attempt at predicting surface wettability via a machine learning method that considered both surface topography and surface chemistry data as the input.

3.1. Experiments

The nHSN process comprises two sequential steps: (1) laser surface process uses a nanosecond pulse laser raster scanning the target material surface under water containment; (2) chemical immersion treatment (CIT), during which the laser-treated surface was chemically functionalized to attach chemical functional group on the textured surface. As shown in Fig. 3, two sets of nHSN processing parameters are used to manipulate the surface attributes: the laser surface processing parameters,

namely laser power intensity, scanning speed and overlap ratio, etc. are controlled to mainly adjust the surface topography, while the chemical immersion treatment parameters are selected to modify the surface chemistry. It should be noted that a novel etching effect of the chlorosilane reagent could generate nanostructures on the laser-treated metal surface. Two common metal alloys, namely aluminum alloy 6061 (AA6061) and steel alloy AISI4130, were used as the substrate materials. 60 samples of AA6061/AISI4130 were treated using different laser power intensities ranging from 0.1 GW/cm² to 8.4 GW/cm², while other laser parameters, including laser beam diameter and pulse width, were kept as the same. For this study, four types of silane solutions were used in the CIT step to achieve extreme wettability, including 1H,1H,2H,2H-perfluorooctyltrichlorosilane [CF₃(CF₂)₅(CH₂)₂SiCl₃] (FOTS), 1H,1H,2H,2H-perfluorodecyltrichlorosilane [CF₃(CF₂)₇(CH₂)₂SiCl₃] (FDTS), 1H,1H,2H,2Hperfluorododecyltrichlorosilane [CF₃(CF₂)₉(CH₂)₂SiCl₃] (FDDTS), and 3cyanopropyltrichlorosilane [CN(CH₂)₃SiCl₃] (CPTS). The functional groups in chlorosilane led to different wettability, that is superhydrophobicity for FOTS/FDTS/FDDTS and superhydrophilicity for CPTS. During the CIT process, the concentration of the solution and the chemical treatment time were kept the same (1.5 wt%). Laser processing and the following chemical treatment conditions of AA6061 and AISI4130 samples are listed in Table 1.

After the fabrication, contact angle measurements were performed using a Rame-Hart model 100 contact angle goniometer at ambient temperature and relative humidity of 50%. During the contact angle measurement, 4 μ L water droplet was micro-pipetted on the treated surface. For each specimen, six measurements were obtained at different locations, and the average value was recorded as the static water contact angle (θ_w), which was then used as the output data for the machine learning algorithm.

3.2. Surface topography data collection and processing

Surface topological features of nHSN treated samples of AA6061 and AISI 4130 alloys were evaluated using a Hitachi S-4800 SEM system. At relatively low magnifications, as shown in Fig. 4a1-3a3for AA 6061 and Fig. 4 s1-3s3 for AISI 4130, respectively, with a view area from thousands of μm^2 up to 1 mm^2 , the nHSN specimen exhibits an isotropic texture with numerous tiny pores homogenously distributed in the

Table 1Laser processing and chemical treatment conditions for AA6061 and AISI4130 samples.

Substrate material	Power intensity (GW/cm ⁻²)	Chemical reagent used in following CIT process
AISI4130	0.1, 0.15, 0.2, 0.3, 0.4, 0.5, 0.6,	FOTS, CPTS
	0.9, 1.3, 1.7, 2.4, 5.4, 8.4	
AA6061	0.2, 0.3, 0.4, 0.5, 0.6, 0.9, 1.3, 1.7,	FOTS, CPTS
	2.4, 5.4, 8.4	
AA6061	0.6, 0.9, 1.3, 2.4, 5.4, 8.4	FDTS, FDDTS

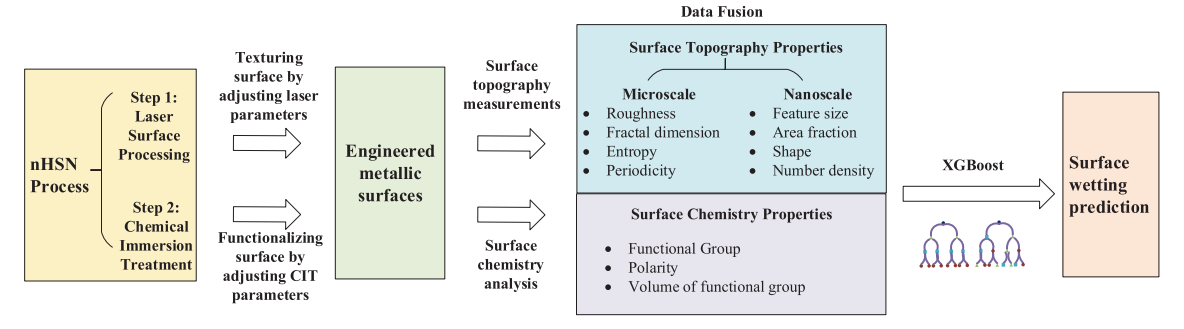


Fig. 3. Case study: machine learning model for nHSN treated surfaces.

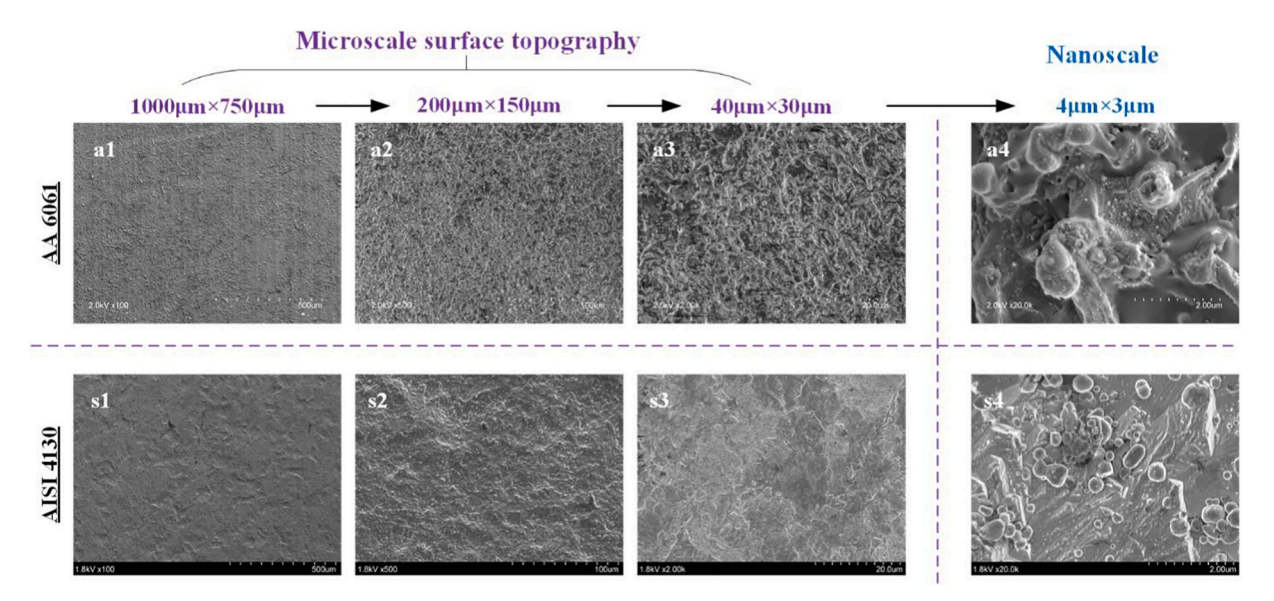


Fig. 4. SEM micrographs of nHSN surfaces at a length scale ranging from hundreds of microns to nanoscale for AA 6061 and AISI 4130 alloys. At microscale areas (a1-a3 for AA 6061 and s1-s-3 for AISI 4130), an isotropic texture without any laser processed pattern is observed. At nanoscale areas (a4 for AA 6061 and s4 for AISI 4130), random nanoscale surface features of ripples, particles, and pores can be seen.

treated area, but no obvious microscale patterns can be observed. At a $20,000\times$ magnification, SEM micrographs for both AA 6061 and AISI 4130 are characterized by nanoscale surface features of ripples, particles, and pores, ranging in size from less than 100 nm to several hundred nm, randomly and closely packed in a view area of several μ m².

Given the randomly nanostructured topography by nHSN, it was a challenging task to define a set of topography parameters which would adequately serve as scale-specific descriptors of the surface topography for the ML model input. For the microscale topography, the nHSN treated samples were first quantified by surface roughness measurement over an evaluation length of a few millimeters. Arithmetical mean roughness R_a was measured using a Taylor Hobson Surtronic 25 profilometer. For each specimen, nine measurements were taken at different locations to obtain the average value. However, profile or areal roughness parameters alone would not be adequate to describe the surface topographic features, particularly for laser surface texturing and patterning processes. Therefore, besides the surface roughness characterization, three other parameters were introduced for the first time, which would be obtained by running computational algorithms to the microscale SEM micrographs, to describe the topographic complexity and randomness of the nHSN surface, viz. fractal dimension (D_f) , twodimensional entropy (H_{2D}) , and periodicity (P_f) . The novelty and significance of introducing these parameters are discussed in the later segments of this section.

In order to extract information of the nanoscale features from the nanoscale SEM micrographs, four nanoscale topography parameters were introduced to describe the shape and size of the nanostructure, viz. average size (A_a), area fraction (F_a), number density (n_f), and circularity (C_f). The ImageJ software was used to process the nanoscale SEM images to extract these attributes. The original SEM image was converted into an 8-bit image using ImageJ at first. After the threshold adjustment and hole filling process, the aforementioned four parameters were computed automatically. These data were then collected as part of the input of the machine learning model. The four nanoscale parameters, together with the four microscale parameters, provide a comprehensive description of the surface morphology. These surface topography parameters are summarized in Table 2.

Fractal dimension is a ratio providing a statistical index of complexity related to self-similarity and irregularity of fractals. In recent years, fractal dimension has been increasingly applied to establish correlations between surface structure and performance, e.g., electrical

 Table 2

 Parameters of surface topography as ML mode input.

Length scale	Parameter	Definition
Microscale (hundreds to tens of μm)	R_a	The arithmetic average value of all absolute distances of the roughness profile from the center line within the measuring length.
	D_f	Fractal dimension is an intrinsic property of the surface that reflects the complexity of the surface structure. D_f is calculated for the SEM images by Shifting Differential Box-Counting method.
	H_{2D}	Two-dimensional entropy of the SEM images, which is a statistical measure of randomness that can be used to characterize the surface texture.
	P_f	The periodicity level of the microstructures in terms of spatial distribution. P_f is calculated based on autocorrelation and discrete Fourier transform.
Submicron &	A_a	Average area of each nanoscale feature.
nanoscale	F_a	The percentage of pixels in the image that has been selected as nanoscale features.
	n_f	Number of the features per unit area.
	C_{f}	The average of $4\pi \times [Area]/[Perimeter]^2$ for
		the nanostructures, with a value of 1.0
		indicating a perfect circle. As the value approaches 0.0, it indicates an increasingly
		elongated shape.

contact resistance [39]. The relationship between fractal dimension and surface wettability was occasionally investigated in the literature. Shibuichi et al. [40] experimentally studied the contact angle of the fractal surface and its relation with the contact angle of the flat surface. Nevertheless, such a relationship only focused on the impact of fractal geometry on surface wettability without taking into account other parameters such as surface chemistry; thus, its application is highly limited. In this work, fractal dimension was used as a surface descriptor indicating the complexity and self-similarity of the laser-induced surface texture, as well as an input feature for the machine learning algorithm.

The shifting differential box-counting (SDBC) method [47] was adopted in this study to compute the fractal dimension of nHSN SEM micrographs, which is an improvement of the well-known differential box-counting (DBC) method [48]. In the DBC method, a 2D gray-level

image of size $M \times M$ pixels is scaled down to a size $s \times s$, which means the image plane (x, y) is covered by a 3D grid of boxes with a grid size s. The number of boxes N_r , containing at least one pixel of the image is counted, and the fractal dimension D_f is then estimated by measuring the slope of the straight line fitting the points $[-\log r, \log N_r]$, i.e.,

$$D_f = -\frac{logN_r}{logr} \tag{1}$$

where the scaling ratio r is estimated by $\frac{s}{M}$. The major shortcoming of this approach is that N_r is not exactly the least number of boxes of side s needed to cover the fractal intensity surface. Herein the SDBC method solves this problem by shifting the boxes along the z direction. The number of boxes counted by SDBC method N_r ' is closer to the exact number of boxes than N_r computed by the DBC method. Hence SDBC method can not only achieve the estimated values of fractal dimension closer to the precise values than the DBC and other box-counting methods [47], but also give more consistent results than the traditional DBC algorithm, and therefore is a reliable approach to get fractal dimension on textured images [49]. Using this method, the micro-/ nano-textured surface is characterized by $2 < D_f < 3$. A fractal surface typically has irregularities that fill the embedding space ($D_f = 3$); thus, it must occupy intrinsically more space than a plane space ($D_f = 2$). Fractal dimension quantifies the disorder in terms of the space-filling ability of the surface [50], which is why it is used in this study to describe the surface morphology.

Hundreds of nHSN surface SEM micrographs of a typical length scale of dozens to hundreds of μm were processed via the SDBC method to

determine the fractal dimension. Typical SEM micrographs of these surface topography examples are shown in Fig. 5a (third row for nHSN treated AISI 4130 and fourth row for nHSN treated AA 6061). Other ultrashort laser-based surface-texturing methods in the literature rely on the generation of microscale patterns (first row of Fig. 5a) or LIPSS (second row of Fig. 5a). These ultrashort laser-based surface-texturing methods scan the surface area using a focused laser spot (often in the range of 30-50 µm) and an excellent spatial resolution. Hence, the resultant surface topological features are very structured in the local area. For the laser microscale patterned surfaces such as cross-hatched pattern [44], grating pattern [45], and rose petal structure [51], the typical surface roughness and feature size are all around dozens of microns. As long as the image size is about hundreds of microns or greater, sufficient features are captured, and a clear pattern is shown. In this case, the fractal dimension values of the patterned surfaces are relatively low, usually smaller than 2.4. Using ultrashort pulsed lasers such as femtosecond [46] and picosecond lasers [52], LIPSS can be generated with a typical surface roughness of dozens of microns to a few microns. The formation of LIPSS can be attributed to the interference of incident and scattered waves [53]. Typically, the incident laser beam has a wavelength of hundreds of nanometers. LIPSS with a spatial period shorter than half of the incident beam wavelength is referred to as highspatial-frequency LIPSS, whereas LIPSS with a period slightly shorter or close to the wavelength is referred to as low-spatial-frequency LIPSS [54]. In the case of LIPSS, the image size of dozens of microns is already enough to show the features. As Fig. 5b shows, the fractal dimension values of LIPSS are higher than the regularly patterned surface,

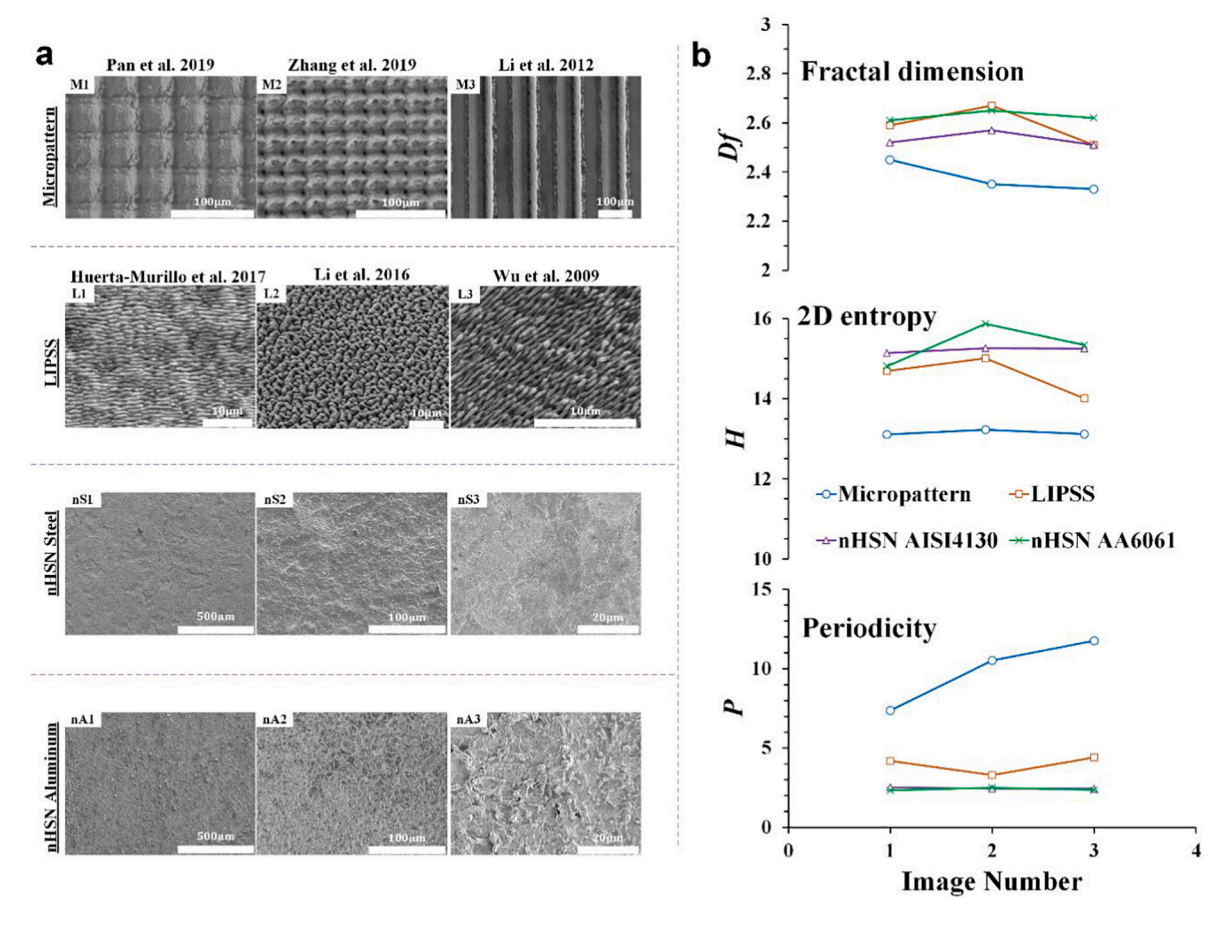


Fig. 5. Microscale topography and parameters for various laser-textured superhydrophobic metallic surfaces by nHSN and in literature [41–46]. (a) SEM images of laser-textured surface: the first row is micropatterned surface; the second row is LIPSS; the third row is AISI 4130 surface produced by nHSN process; the fourth row is AA6061 surface produced by nHSN process; (b) Fractal dimension, 2D entropy, and periodicity results. D_f is calculated for the SEM images by Shifting Differential Box-Counting method. 2D entropy H_{2D} is a statistical measure of randomness that can be used to characterize the surface texture. Periodicity level P_f of the microstructures in terms of spatial distribution and is calculated based on autocorrelation and discrete Fourier transform.

indicating that LIPSS occupies the embedding space more compactly [55]. For our nHSN surfaces, however, on a similar scale (from dozens of microns to hundreds of microns), the surface structures are all random and featureless for both AISI4130 and AA6061 samples. The fractal dimension values are higher than the micropatterned surface, which indicates that the surface structure generated by the nHSN process is less rough (surface roughness less than 1 μm) and has more space-filling irregularities [50]. Moreover, the AA6061 surfaces have greater fractal dimension values than the AISI4130 surfaces, showing that there is a slight difference in the surface structure between the two materials.

Image entropy was used as another input feature of the machine learning algorithm to describe the level of randomness of the surface structures. The well-known Shannon entropy has been applied to quantitatively measure the randomness of the gray-level distribution of images for decades [56,57]. As Shannon entropy accounts only for individual pixels occurrence and no spatial structure is taken into account [58], it is not capable of comparing the randomness of the surface structure. Herein, a two-dimension entropy [59] was adopted in this work to analyze the surface structure, which is an extension to the traditional 1D Shannon entropy. In this approach, the spatial correlation between the pixels in an image is taken into account. Consider an image with N \times N pixels, the total number of occurrence, f_{ii} , of a pair (i, j)divided by the total number of pixels, N^2 , defines the joint probability mass function, p_{ij} : viz., $p_{ij} = f_{ij}/N^2$, where i is the gray value of a pixel (0 $\leq i \leq 255$), and j is the average gray value of the pixels adjacent to that pixel (0 \leq j \leq 255). Then the 2D entropy is defined as:

$$H_{2D} = -\sum_{i=0}^{255} \sum_{i=0}^{255} p_{ij} log_2 p_{ij}$$
 (2)

When all the images are scaled down to the size of 256×256 pixels, the 2D entropy value is within the range from 0 to 16, while the greater entropy value represents higher randomness. Frankly speaking, limitations exist as the image with a high entropy value may not be necessarily random-like [60]. However, 2D entropy still provides useful information to some extent regarding the randomness of the spatial structure. To the best knowledge of the authors, 2D entropy so far has not been widely applied to materials research. This work will provide insight into the engineering application of 2D entropy.

2D entropy was also computed on SEM images of the micropatterned surface, LIPSS, and nHSN surfaces. The results showed that the laser micropatterned surfaces have the lowest entropy in the range of 13–14, which is related to the relatively low randomness in microscale surface texture. The entropy of LIPSS is higher (14–15), as the feature in LIPSS is periodic but a little more chaotic than the highly patterned surface in terms of spatial distribution. For the nHSN sample, as expected, the highest entropy is obtained (>15) since the nHSN structure is highly random in microscale. AA6061 surfaces have slightly higher entropy than AISI4130, which indicates that the AA6061 surfaces have higher randomness in spatial structure.

For laser-textured surfaces, periodicity is usually defined as the average distance between the neighboring structures [61,62], especially for LIPSS [63,64]. For nHSN samples, however, the spatial distribution of the surface structure is irregular and relatively random. In this case, a quantitative method to describe its degree of periodicity was introduced to better describe the spatial distribution of the surface structure in a microscale. In this study, the periodicity of the surface structure was computed based on autocorrelation and Fourier transform. Autocorrelation function has been widely used as the basis of the texture characterization [65] since it has the same cyclic characteristics as the original signal. The procedure of extracting the periodicity of the surface texture is described as follows. First of all, a template window is selected randomly. Then the normalized cross-correlation of the template and the whole image is computed to extract the periodic signal obscured by noise. After that, the discrete Fourier transform is performed onto the normalized correlation coefficient matrix. The maximum peak value of the Fourier transform, which represents the magnitude of the main periodic component, is then determined as the periodicity (P_f) of the surface texture, viz.

$$P_f = max[peaks(DFT(autocorrelation(template, image)))]$$
 (3)

The periodicity here is a non-dimensional parameter that gives a number greater than zero, as the larger values represent higher periodicity. Typically, a periodicity value less than three indicates a random surface structure, while a periodicity value larger than three indicates that periodic structures exist.

Periodicity extraction was also performed on the SEM images, as shown in Fig. 5b. As expected, the micropatterned surfaces and LIPSS have the greatest periodicity. The nHSN surfaces, on the contrary, all have a low periodicity value (<3), which is in accordance with the high randomness of the surface structure generated by the nHSN process. The periodicity value of LIPSS lies in between, as there are periodic structures present on LIPSS surfaces, but the structures are not as regular as other patterned surfaces.

3.3. Surface chemistry data collection and processing

Surface chemical composition of nHSN surfaces was analyzed using a Kratos Axis Ultra high-performance XPS system with an Al Kα (1486.6 eV) line excitation source. Both survey spectrum analysis and core-level spectrum analysis were performed. Fig. 6 shows two typical XPS spectra of AA6061 samples treated with FOTS and CPTS, respectively. The samples treated with FDTS and FDDTS would show similar spectra as the samples treated with FOTS since FOTS contains the same functional groups as FDTS and FDDTS. According to the XPS spectra shown in Fig. 6, the -CF₃, -CF₂-, and -C \equiv N peaks confirmed the existence of FOTS and CPTS, respectively. In literature, binding energies were usually used as the input features for the machine learning algorithms [66,67]. In our case study, however, the binding energy is not a suitable feature to be extracted as there is no clear evidence showing that the binding energy is correlated with surface wettability. It would only act as a label indicating the type of chemicals, not as a meaningful scalar that has a correlation with θ_w . Peak area under the curve, on the other hand, represents the concentration of chemicals. The relative percentage of each functional group can be obtained by dividing its peak area by the total area formed by the different functional groups of the same element [68]. Therefore, the peak area fraction was chosen as the input feature of the machine learning algorithm.

With the surface chemical composition identified via XPS analysis, a set of surface chemistry parameters were introduced in this study to describe the physicochemical properties of the functional groups as the ML model input. According to Dalvi et al. [69], the wetting behavior of the fluorocarbon is not only related to the molecular polarity but also related to the size of the surface reagent molecules, which will influence the van der Waals interactions between the reagent and the liquid. Thus, the dipole moment and volume of the most dominant functional group present on the surface were introduced as the other two input features. In this study, the most dominant functional group was determined as -CF2 for samples treated with FOTS, FDTS, or FDDTS, and as -CN for samples treated with CPTS. Table 3 summarizes the chemistry parameters used for the machine learning model.

3.4. Learning using XGBoost

The XGBoost model was adopted in this work to learn. The concept of XGBoost developed by Chen et al. [32] is often considered one of the best off-the-shelf machine learning models in recent years. In general, the XGBoost follows the principle of gradient boosting with a more regularized model formulation to control overfitting, which leads to better performance. Gradient boosting is a sequential technique combining a bunch of weak learners to give improved predictions. In XGBoost, a similar "additive strategy" is used. An ensemble of regression

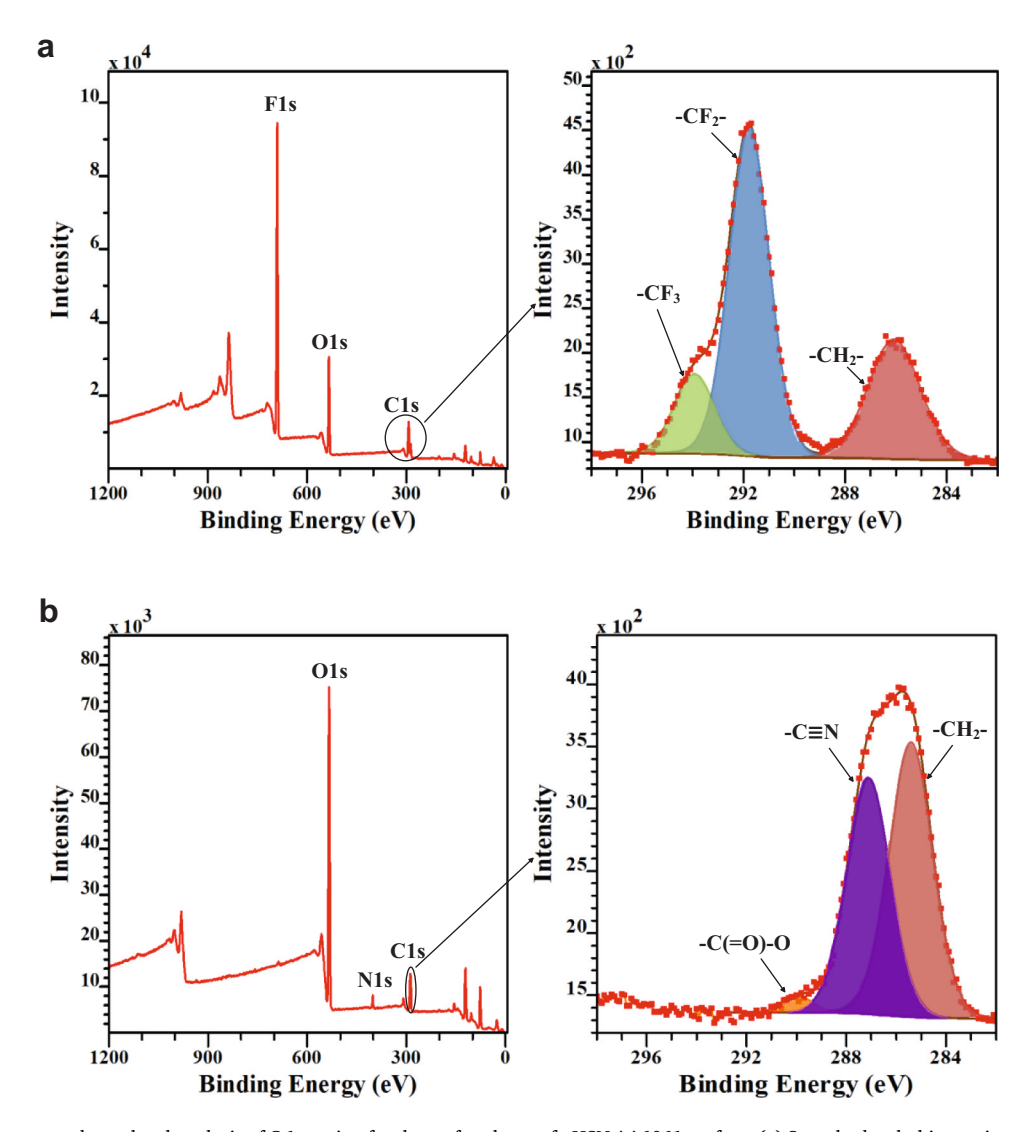


Fig. 6. XPS survey spectra and core level analysis of C 1s region for the surface layer of nHSN AA6061 surface. (a) Superhydrophobic specimen; (b) Superhydrophilic specimen. The peak area fraction P_{AF} is denoted for the dominant functional group in the XPS C1s spectrum.

Table 3Surface chemistry parameters for ML model input.

Parameter	Definition
P_{AF}	The peak area fraction of the most dominant functional group in the XPS C1s spectrum.
μ $V_{ m g}$	The dipole moment of the most dominant functional group in Debye. The volume occupied by the most dominant functional group, in \mathring{A}^3 .

trees is grown one after another. Each subsequent tree attempts to reduce the misprediction error of the previous tree. The results of all the trees are added together to deliver the final prediction. XGBoost uses additional regularization terms to improve performance in comparison with the traditional gradient boosting algorithm. Specifically, XGBoost tries to minimize the regularized objective as the following [70].

$$L = \sum_{i} l(\widehat{y_i}, y_i) + \sum_{k} \Omega(f_k), \text{ where } \Omega(f) = \gamma T + \frac{1}{2} \lambda ||\omega||^2$$
 (4)

where l is the loss function as a measure of the difference between the predicted outputs $\hat{y_i}$ and the actual outputs y_i , f_k is the kth regression tree in the ensemble model, and Ω is the regularization term to penalize the complexity of the model in terms of T, the number of leaves in a tree, and

 ω , the vector of scores on leaves. This regularization term turned out to be very helpful and gave better performance compared with the traditional gradient boosting algorithm.

In this case study, the input data was standardized first by subtracting the mean value for each feature and then dividing the values by the standard deviation. The 'feature' here does not mean the surface texture micro- or nano-features anymore. Instead, it is a statistical concept meaning an individual measurable property (in our case, an input variable such as D_f). After the standardization of the data, 57 trees in total were grown following the XGBoost algorithm to learn. Since the data size was relatively small in this case study, a hold-out method splitting the data set into a test set and a training set is not efficient. Hence a 12-fold cross-validation method was used to evaluate the machine learning model. The procedure was described as follows: (1) shuffle the dataset randomly; (2) split the dataset into twelve groups, each of which contained five samples; (3) took one of the groups as the test set, while the remaining groups were taken as the training set; (4) fit the model on the training set and evaluated it on the test set; (5) recorded the evaluation score (root mean squared error) and then discarded the model; (6) repeated steps (1)-(5) for all twelve groups and average the evaluation scores. By this method, each sample was given the opportunity to be used in the test set for once and used to train the model eleven times, which provided the maximum use of the data to improve efficiency in model performance evaluation.

4. Results & discussion

In order to obtain better training data characteristics, the Pearson correlation coefficients between different features were calculated and expressed as a heatmap, as shown in Fig. 7. The Pearson correlation coefficient described the linear correlation between two features. When two features have a strong linear correlation with each other, one feature can be expressed by the other, and the information contained by these two features has no distinct difference. Therefore, for two features with strong linear correlation, removing one of them is necessary to enhance the model performance. According to the heatmap, some data redundancy was revealed, especially for the chemistry features. That is due to the small size of the dataset employed in this work. Only four different types of chemical reagents were used for the CIT process, three of which contained the same functional groups, and therefore, many chemistry variables chosen here were highly related to each other. For this case study, the redundant features were removed that had a Pearson correlation coefficient greater than 0.9 with other features. Eight features remained were used as the input, viz. R_a , D_f , P_f , H_{2D} , n_f , A_a , P_{AF} , and μ . However, it is noted that the redundant features determined in this work may still be useful for future work involving larger datasets. In fact, these features would be very useful when more chemicals are considered for future research.

4.1. Role of surface chemistry

The root mean squared error (RMSE) from the cross-validation was used to evaluate the model. The RMSE is defined as $RMSE = \sqrt{\frac{1}{n}\sum_{i=1}^{n}\left(\hat{y_i}-y_i\right)^2}$, where $\hat{y_i}$ is the predicted value, y_i is the observed value, and n is the number of samples. RMSE has the same unit as the output variable, which makes the evaluation result more intuitive. By parameter tuning, the maximum tree depth was set as 5, the boosting learning rate was 0.1, and the regularization term was 1. The results showed that the RMSE of this model was 18.53 without feature selection and was reduced to 17.94 after feature selection. In comparison, the RMSE of a linear regression model was 23.22 after feature selection. The XGBoost generated a more accurate prediction, with a 23% reduction of prediction error. Furthermore, the goodness of fit of a linear regression

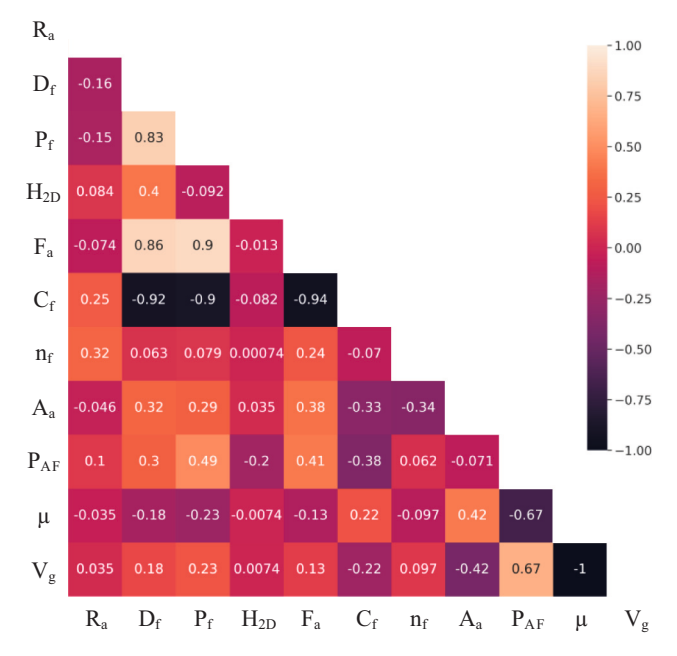


Fig. 7. Heatmap of Pearson correlation coefficient matrix.

model was checked, showing a non-random zigzag pattern in the residual plot, which indicates that some of the essential complex patterns exist in the data and cannot be captured by the linear regression model. Therefore, the complexity of the data requires a more sophisticated model such as XGBoost. The residuals of XGBoost exhibit mostly a random pattern, indicating that the model is much more adequate for the surface wettability prediction problem.

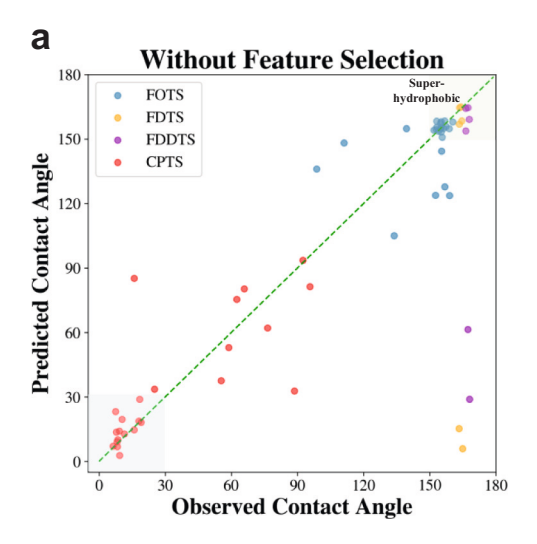
The comparison between the predicted water contact angle by the XGBoost model and the true water contact angle (Fig. 8) showed a decent match. From the results, we can see that the XGBoost has the ability to handle the wettability prediction problem even if the data size is small. Fig. 8 also showed a clear classification of contact angle according to the chemical reagent type. All the samples treated with CPTS are located in the lower-left quarter, which is the hydrophilic region, and the other samples treated with FOTS/FDTS/FDDTS are located in the upper right quarter, which is the hydrophobic region, no matter what surface structures they have. Therefore, according to the dataset obtained from the experiments, it can be seen that surface chemistry is the dominant factor here in the determination of whether the sample is hydrophobic or hydrophilic.

XGBoost is also capable of examining the importance of each feature in the dataset. The feature importance analysis was performed, and all the features were sorted in the order of 'Gain,' which is the average information gain across all splits the feature is used. The information gain is well used in machine learning and is defined as the amount of information provided by the features [71]. A higher value of gain, when compared to another feature, indicates it is more important for generating a prediction.

As Fig. 9 shows, the polarity of the functional group (μ) and its relative amount (P_{AF}) are the two most important features in determining the wettability, which is consistent with the knowledge gained from the contact angle prediction results. The surface chemistry plays a decisive role in the determination of whether the surface is hydrophobic or hydrophilic, while the surface morphology only plays a supporting role in tuning the contact angle in a relatively small range without switching its wetting behavior between hydrophobicity and hydrophilicity. In addition, the water contact angle showed a strong negative correlation with the dipole moment of the functional group (Pearson's r value = -0.93). Since V_g is negatively related with μ in this dataset, as shown in the heatmap, the water contact angle would have a positive correlation with the volume of the functional group. The results provide guidance for engineers to fabricate metal surfaces with desired wettability. If a hydrophobic surface is wanted, the most important thing to do is to apply functional groups with small dipole moment and large volume onto the surface instead of spending too much effort texturing the surface to achieve desired surface structure. On the other hand, it is important to point out that the results are highly dependent on the dataset. Since the dataset in this case study is small, the results are biased towards the importance of chemistry. When more data are incorporated into the dataset in the future, the feature importance analysis will give a more objective estimation. If the polarity was the only input feature used for prediction in this case study, a decent match could still be acquired (RMSE = 21.01). However, the results would not be expandable to explain the wetting phenomena for other types of surfaces.

4.2. Role of surface topography

Since the chemistry feature established its dominance for the water contact angle prediction in this case study, it shadowed all the other features to some extent. In order to investigate the importance of other surface morphology and roughness features, only the samples treated with superhydrophobic chemicals (FOTS/FDTS/FDDTS) were selected as a data subset. The surface chemistry did not show much difference within this subset. The feature importance analysis was then performed on this subset.



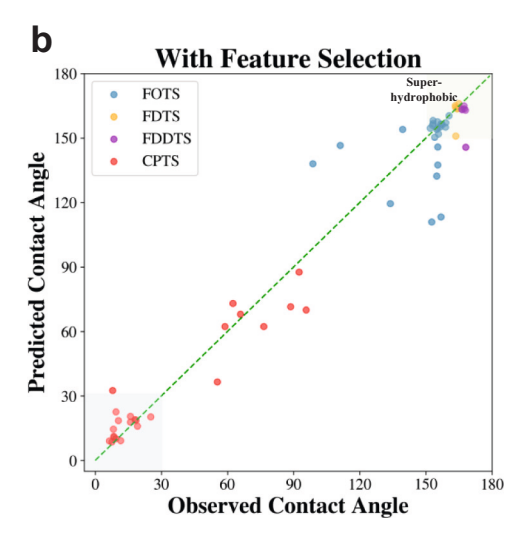


Fig. 8. The prediction of water contact angle by XGBoost in comparison with the ground truth data (a) before feature selection; (b) after feature selection.

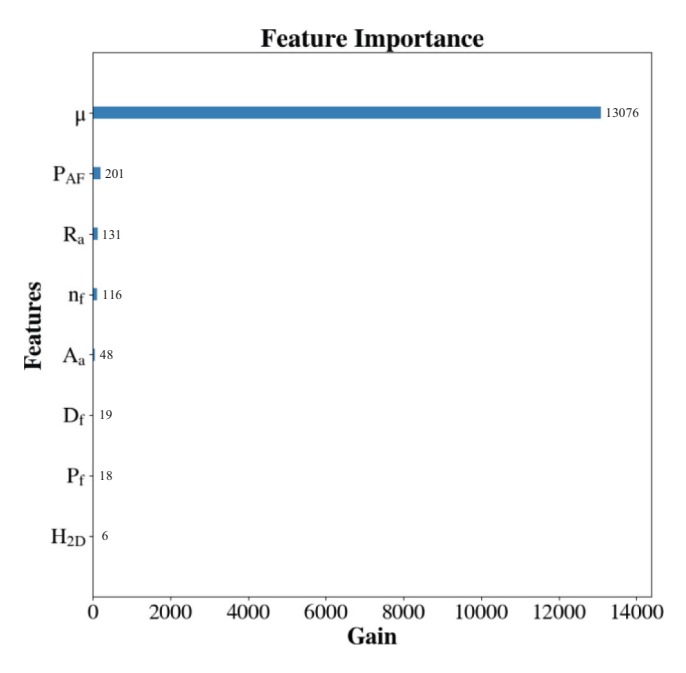


Fig. 9. Feature importance in terms of information gain.

Fig. 10 shows the features adopted by the XGBoost model for the prediction of the contact angle and their importance ranking for the three data subsets. It can be seen that the nanostructure, roughness, as well as the relative amount of functional groups play the most critical roles in the determination of the final wettability, while the microstructure does not influence the $\theta_{\rm w}$ too much. This indicates that when fabricating metal surfaces with different wetting behavior, surface patterning is relatively trivial as long as certain roughness and nanostructures are achieved. As shown previously, nHSN surface with random microstructure and patterned surface with periodic microstructure can all achieve superhydrophobicity or superhydrophilicity. Again, it needs to be noted that the data size was small in this case study, and the feature importance analysis performed by the XGBoost model also has uncertainty. In order to extend the results to wider applications, more data needs to be incorporated in the future.

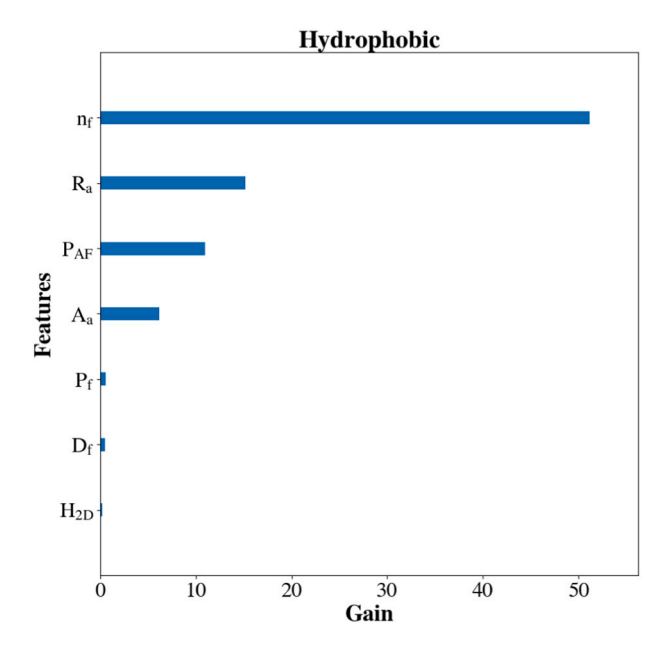


Fig. 10. Feature importance ranking for the hydrophobic surface.

5. Conclusion and recommendation

In this paper, a general machine learning framework of surface wetting was proposed by considering a broad range of factors, including solid surface topography, solid surface chemistry, liquid properties, and environmental conditions. A specific XGBoost-based ML model was presented for learning the wetting behavior of nHSN treated surfaces to water under lab-controlled environments. The novelty and significance of this research are the following:

- It was the first attempt to develop a machine learning model considering both surface topography and surface chemistry properties to predict surface wettability.
- 2) Novel microscale and nanoscale topography parameters were defined with suitable computer algorithms to comprehensively describe the surface topography, which includes fractal dimension, 2D entropy, and periodicity.

- Novel surface chemistry parameters such as polarity, volume, and amount of functional groups were used as the machine learning model input.
- 4) The feature importance results showed that the surface chemistry is the dominant feature affecting the wetting behavior of the nHSN processed metal surface. The secondary role of the surface topography, i.e., nanostructure and surface roughness, was also established for nHSN surfaces.

It is noted that the ML modeling results are restricted to the nHSN process, during which either superhydrophobic or superhydrophilic functionalization is resolutely designed and highly effective. Caution should be exercised to apply these findings to other surface modification processes to achieve a superhydrophobic surface. Although the current dataset has a limited size, it is worth noting that proposing an ML approach to predict surface wetting behavior is promising, as the input dataset is readily expandable, and a larger dataset with more types of variables can be incorporated as the input/output variables, such as environmental parameters (e.g., temperature, pressure, and humidity), liquid properties (e.g., viscosity and polarity), and other measurements of wettability (e.g., roll-off angle and surface energy). Process-specific parameters can also be added to the ML approach to help obtain the process-surface-wetting relationship. With the same machine learning algorithm being used, this approach can be applied to a wider situation of wettability prediction and provide design guidance for engineers when they are trying to manufacture surfaces with certain wettability.

Declaration of competing interest

The authors declare that they have no known competing financial interests or personal relationships that could have appeared to influence the work reported in this paper.

Acknowledgements

The authors gratefully acknowledge the financial support by the National Science Foundation under grants CMMI-1762353 and DCL Data Science Activities for the Civil, Mechanical, and Manufacturing Innovation Communities.

References

- [1] Moldoveanu SC, David V. RP-HPLC analytical columns. 2017. doi:https://doi. org/10.1016/b978-0-12-803684-6.00007-x.
- [2] McHale G, Shirtcliffe NJ, Aqil S, Perry CC, Newton MI. Topography driven spreading. Phys Rev Lett 2004;93:36102. https://doi.org/10.1103/ PhysRevLett.93.036102.
- [3] Hay KM, Dragila MI, Liburdy J. Theoretical model for the wetting of a rough surface. J Colloid Interface Sci 2008;325:472–7. https://doi.org/10.1016/j. icis.2008.06.004.
- [4] Samanta A, Huang W, Chaudhry H, Wang Q, Shaw SK, Ding H. Design of chemical surface treatment for laser textured metal alloy to achieve extreme wetting behavior. ACS Appl Mater Interfaces 2020;12:18032–45. https://doi.org/10.1021/ acsami.9b21438.
- [5] Samanta A, Wang Q, Shaw SK, Ding H. Roles of chemistry modification for laser textured metal alloys to achieve extreme surface wetting behaviors. Mater Des 2020:192:108744–1–25.
- [6] Chau TT, Bruckard WJ, PTL Koh, Nguyen AV. A review of factors that affect contact angle and implications for flotation practice. Adv Colloid Interface Sci 2009;150: 106–15. https://doi.org/10.1016/j.cis.2009.07.003.
- [7] Busscher HJ, van Pelt AWJ, de Boer P, de Jong HP, Arends J. The effect of surface roughening of polymers on measured contact angles of liquids. Colloids Surf 1984; 9:319–31. https://doi.org/10.1016/0166-6622(84)80175-4.
- [8] Veeramasuneni S, Drelich J, Miller JD, Yamauchi G. Hydrophobicity of ion-plated PTFE coatings. Prog Org Coat 1997;31:265–70. https://doi.org/10.1016/S0300-9440(97)00085-4.
- [9] AlRatrout A, Blunt MJ, Bijeljic B. Wettability in complex porous materials, the mixed-wet state, and its relationship to surface roughness. Proc Natl Acad Sci U S A 2018;115:8901–6. https://doi.org/10.1073/pnas.1803734115.
- [10] Belaud V, Valette S, Stremsdoerfer G, Bigerelle M, Benayoun S. Wettability versus roughness: multi-scales approach. Tribol Int 2015;82:343–9. https://doi.org/ 10.1016/j.triboint.2014.07.002.

- [11] Ahuir-Torres JI, Arenas MA, Perrie W, Dearden G, de Damborenea J. Surface texturing of aluminium alloy AA2024-T3 by picosecond laser: effect on wettability and corrosion properties. Surf Coat Technol 2017;321:279–91. https://doi.org/ 10.1016/j.surfcoat.2017.04.056.
- [12] Jiao Y, Brousseau E, Shen X, Wang X, Han Q, Zhu H, et al. Investigations in the fabrication of surface patterns for wettability modification on a Zr-based bulk metallic glass by nanosecond laser surface texturing. J Mater Process Technol 2020;283:116714. https://doi.org/10.1016/j.jmatprotec.2020.116714.
- [13] Granados E, Calderon MM, Krzywinski J, Wörner E, Rodriguez A, Aranzadi MG, et al. Enhancement of surface area and wettability properties of boron doped diamond by femtosecond laser-induced periodic surface structuring. Optical Materials Express 2017;7:3389–96.
- [14] Khorkov KS, Kochuev DA, Dzus MA, Prokoshev VG. Wettability surface control on stainless steel by LIPSS formation. In: J Phys Conf Ser. IOP Publishing; 1822–2021. p. 12010.
- [15] Batal A, Michalek A, Garcia-Giron A, Nasrollahi V, Penchev P, Sammons R, et al. Effects of laser processing conditions on wettability and proliferation of Saos-2 cells on CoCrMo alloy surfaces. Adv Opt Technol 2020;9:67–78. https://doi.org/ 10.1515/aot-2019-0051.
- [16] Orazi L, Gnilitskyi I, Serro AP. Laser nanopatterning for wettability applications. J Micro Nano-Manufacturing 2017:5.
- [17] Liang CJ, Liao JD, Li AJ, Chen C, Lin HY, Wang XJ, et al. Relationship between wettabilities and chemical compositions of candle soots. Fuel 2014;128:422–7. https://doi.org/10.1016/j.fuel.2014.03.039.
- [18] Pan Y, Kong W, Bhushan B, Zhao X. Rapid, ultraviolet-induced, reversibly switchable wettability of superhydrophobic/superhydrophilic surfaces. Beilstein J Nanotechnol 2019;10:866–73. https://doi.org/10.3762/BJNANO.10.87.
- [19] Psarski M, Pawlak D, Grobelny J, Celichowski G. Relationships between surface chemistry, nanotopography, wettability and ice adhesion in epoxy and SU-8 modified with fluoroalkylsilanes from the vapor phase. Appl Surf Sci 2019;479: 489–98. https://doi.org/10.1016/j.apsusc.2019.02.082.
- [20] Zhang J, Han Y. A topography/chemical composition gradient polystyrene surface: toward the investigation of the relationship between surface wettability and surface structure and chemical composition. Langmuir 2008;24:796–801. https://doi.org/10.1021/la702567w.
- [21] Zhang D, Cheng Z, Kang H, Yu J, Liu Y, Jiang L. A smart superwetting surface with responsivity in both surface chemistry and microstructure. Angew Chemie 2018; 130:3763–7. https://doi.org/10.1002/ange.201800416.
- [22] Wenzel RN. Resistance of solid surfaces to wetting by water. Ind Eng Chem 1936; 28:988–94.
- [23] Cassie ABD, Baxter S. Wettability of porous surfaces. Trans Faraday Soc 1944;40: 546–51.
- [24] Sun X, Xiao S, Deng H, Hu W. Molecular dynamics simulation of wetting behaviors of Li on W surfaces. Fusion Eng Des 2017;117:188–93. https://doi.org/10.1016/j. fusengdes.2016.06.037.
- [25] Costa D, Arrouvel C, Breysse M, Toulhoat H, Raybaud P. Edge wetting effects of γ-Al2O3 and anatase-TiO2 supports by MoS2 and CoMoS active phases: a DFT study. J Catal 2007;246:325-43. https://doi.org/10.1016/j.jcat.2006.12.007.
- [26] Tanaka I. Nanoinformatics. 2018. doi:https://doi.org/10.1007/978-981-10-7617-
- [27] Yildiz B, Bilbao JI, Sproul AB. A review and analysis of regression and machine learning models on commercial building electricity load forecasting. Renew Sustain Energy Rev 2017;73:1104–22. https://doi.org/10.1016/j. rser.2017.02.023.
- [28] Wu D, Jennings C, Terpenny J, Gao RX, Kumara S. A comparative study on machine learning algorithms for smart manufacturing: tool wear prediction using random forests. J Manuf Sci Eng Trans ASME 2017;139:1–9. https://doi.org/ 10.1115/1.4036350.
- [29] Aly M. Survey on multiclass classification methods. Neural Netw 2005:1-9.
- [30] Drucker H, Surges CJC, Kaufman L, Smola A, Vapnik V. Support vector regression machines. Adv Neural Inf Process Syst 1997;1:155–61.
- [31] Breiman L. Random forests. Mach Learn 2001;45:5–32. https://doi.org/10.1017/ CBO9781107415324.004.
- [32] Chen T, xgboost He T. Extreme gradient boosting. R Packag Version 2015:1–4.
- [33] Song K, Yan F, Ding T, Gao L, Lu S. A steel property optimization model based on the XGBoost algorithm and improved PSO. Comput Mater Sci 2020;174:109472. https://doi.org/10.1016/j.commatsci.2019.109472.
- [34] Wang C, Deng C, Wang S. Imbalance-XGBoost: leveraging weighted and focal losses for binary label-imbalanced classification with XGBoost. Pattern Recog Lett 2020; 136:190-7
- [35] Wang Q, Samanta A, Shaw SK, Hu H, Ding H. Nanosecond laser-based high-throughput surface nanostructuring (nHSN). Appl Surf Sci 2020;507:145136. https://doi.org/10.1016/j.apsusc.2004.11.001.
- [36] Samanta A, Wang Q, Singh G, Shaw SK, Toor F, Ratner A, et al. Nanosecond pulsed laser processing turns engineering metal alloys antireflective and Superwicking. J Manuf Process 2020;54:28–37. https://doi.org/10.1016/j.jmapro.2020.02.029.
- [37] Samanta A, Wang Q, Shaw SK, Ding H. Nanostructuring of laser textured surface to achieve superhydrophobicity on engineering metal surface. J Laser Appl 2019;31: 022515. https://doi.org/10.2351/1.5096148.
- [38] Liu Y, Zhang Z, Hu H, Hu H, Samanta A, Wang Q, et al. An experimental study to characterize a surface treated with a novel laser surface texturing technique: water repellency and reduced ice adhesion. Surf Coat Technol 2019;374:634–44. https:// doi.org/10.1016/j.surfcoat.2019.06.046.
- [39] Zhai C, Hanaor D, Proust G, Gan Y. Stress-dependent electrical contact resistance at fractal rough surfaces. J Eng Mech 2017;143:1–8. https://doi.org/10.1061/(asce) em.1943-7889.0000967.

- [40] Shibuichi S, Onda T, Satoh N, Tsujii K. Super water-repellent surfaces resulting from fractal structure. J Phys Chem 1996;100:19512–7. https://doi.org/10.1021/ is0616779
- [41] Pan Q, Cao Y, Xue W, Zhu D, Liu W. Picosecond laser-textured stainless steel superhydrophobic surface with an antibacterial adhesion property. Langmuir 2019;35:11414–21. https://doi.org/10.1021/acs.langmuir.9b01333.
- [42] Huerta-Murillo D, Aguilar-Morales AI, Alamri S, Cardoso JT, Jagdheesh R, Lasagni AF, et al. Fabrication of multi-scale periodic surface structures on Ti-6Al-4V by direct laser writing and direct laser interference patterning for modified wettability applications. Opt Lasers Eng 2017;98:134–42. https://doi.org/ 10.1016/j.joptlaseng.2017.06.017.
- [43] Li B, Li H, Huang L, Ren N, Kong X. Femtosecond pulsed laser textured titanium surfaces with stable superhydrophilicity and superhydrophobicity. Appl Surf Sci 2016;389:585–93. https://doi.org/10.1016/j.apsusc.2016.07.137.
- [44] Zhang Z, Gu Q, Jiang W, Zhu H, Xu K, Ren Y, et al. Achieving of bionic superhydrophobicity by electrodepositing nano-Ni-pyramids on the picosecond laserablated micro-Cu-cone surface. Surf Coat Technol 2019;363:170–8. https://doi. org/10.1016/j.surfcoat.2019.02.037.
- [45] Li BJ, Zhou M, Zhang W, Amoako G, Gao CY. Comparison of structures and hydrophobicity of femtosecond and nanosecond laser-etched surfaces on silicon. Appl Surf Sci 2012;263:45–9. https://doi.org/10.1016/j.apsusc.2012.08.092.
- [46] Wu B, Zhou M, Li J, Ye X, Li G, Cai L. Superhydrophobic surfaces fabricated by microstructuring of stainless steel using a femtosecond laser. Appl Surf Sci 2009; 256:61–6. https://doi.org/10.1016/j.apsusc.2009.07.061.
- [47] Chen W-S, Yuan S-Y, Hsieh C-M. Two algorithms to estimate fractal dimension of gray-level images. Opt Eng 2003;42:2452. https://doi.org/10.1117/1.1585061.
- [48] Sarkar N, Chaudhuri BB. An efficient approach to estimate fractal dimension of textural images. Pattern Recog 1992;25:1035–41. https://doi.org/10.1016/0031-2203(02)00066 P.
- [49] Liu Y, Chen L, Wang H, Jiang L, Zhang Y, Zhao J, et al. An improved differential box-counting method to estimate fractal dimensions of gray-level images. J Vis Commun Image Represent 2014;25:1102–11. https://doi.org/10.1016/j. ivcir.2014.03.008
- [50] Rosales-Leal JI, Rodríguez-Valverde MA, Mazzaglia G, Ramón-Torregrosa PJ, Díaz-Rodríguez L, García-Martínez O, et al. Effect of roughness, wettability and morphology of engineered titanium surfaces on osteoblast-like cell adhesion. Colloids Surf A Physicochem Eng Asp 2010;365:222–9. https://doi.org/10.1016/j.colsurfa.2009.12.017.
- [51] Jiang W, Mao M, Qiu W, Zhu Y, Liang B. Biomimetic superhydrophobic engineering metal surface with hierarchical structure and tunable adhesion: design of microscale pattern. Indus Eng Chem Res 2017;56:907–19. https://doi.org/ 10.1021/acs.jecr.6b03936.
- [52] Long J, Fan P, Zhong M, Zhang H, Xie Y, Lin C. Superhydrophobic and colorful copper surfaces fabricated by picosecond laser induced periodic nanostructures. Appl Surf Sci 2014;311:461–7. https://doi.org/10.1016/j.apsusc.2014.05.090.
- [53] Sipe JE, Young JF, Preston JS, van Driel HM. Laser-induced periodic surface structure. I. Theory. Phys Rev B 1983;27:1141–54. https://doi.org/10.1103/ PhysRevB.27.1141.
- [54] Hikage H, Nosaka N, Matsuo S. High-spatial-frequency periodic surface structures on steel substrate induced by subnanosecond laser pulses. Appl Phys Express 2017; 10:18–21. https://doi.org/10.7567/APEX.10.112701.

- [55] Mandelbrot BB, Wheeler JA. The fractal geometry of nature. American Journal of Physics 1983;51:286–7. https://doi.org/10.1119/1.13295.
- [56] Akhshani A, Behnia S, Akhavan A, Hassan HA, Hassan Z. A novel scheme for image encryption based on 2D piecewise chaotic maps. Optics Commun 2010;283: 3259–66. https://doi.org/10.1016/j.optcom.2010.04.056.
- [57] Shamir L, Wolkow CA, Goldberg IG. Quantitative measurement of aging using image texture entropy. Bioinformatics 2009;25:3060–3. https://doi.org/10.1093/ bioinformatics/btp571.
- [58] Silva LEV, Filho ACSS, Fazan VPS, Felipe JC, Murta LO. Two-dimensional sample entropy: assessing image texture through irregularity. Biomed Phys Eng Express 2016:2. https://doi.org/10.1088/2057-1976/2/4/045002.
- [59] Abutaleb AS. Automatic thresholding of gray-level pictures using two-dimensional entropy. Comput Vision, Graph Image Process 1989;47:22–32. https://doi.org/ 10.1016/0734-189X(89)90051-0.
- [60] Wu Y, Zhou Y, Saveriades G, Agaian S, Noonan JP, Natarajan P. Local Shannon entropy measure with statistical tests for image randomness. Inf Sci (Ny) 2013;222: 323–42. https://doi.org/10.1016/j.ins.2012.07.049.
- [61] Shimizu M, Sawano H, Yoshioka H, Shinno H. Surface texture assessment of ultraprecision machined parts based on laser speckle pattern analysis. Precis Eng 2014; 38:1–8. https://doi.org/10.1016/j.precisioneng.2013.06.005.
- [62] Shen N, Ding H, Wang Q, Ding H. Effect of confinement on surface modification for laser peen forming without protective coating. Surf Coat Technol 2016:289. https://doi.org/10.1016/j.surfcoat.2016.01.054.
- [63] Romano JM, Garcia-Giron A, Penchev P, Dimov S. Triangular laser-induced submicron textures for functionalising stainless steel surfaces. Appl Surf Sci 2018; 440:162–9. https://doi.org/10.1016/j.apsusc.2018.01.086.
- [64] Raimbault O, Benayoun S, Anselme K, Mauclair C, Bourgade T, Kietzig AM, et al. The effects of femtosecond laser-textured Ti-6Al-4V on wettability and cell response. Mater Sci Eng C 2016;69:311–20. https://doi.org/10.1016/j. msec.2016.06.072.
- [65] Lin HC, Wang LL, Yang SN. Extracting periodicity of a regular texture based on autocorrelation functions. Pattern Recog Lett 1997;18:433–43. https://doi.org/ 10.1016/S0167-8655(97)00030-5.
- [66] Gabourie A, Mcclellan C, Deshmukh S. X-ray photoelectron spectroscopy enhanced by machine learning n.d.:1–6.
- [67] Drera G, Kropf CM, Sangaletti L. Deep neural network for x-ray photoelectron spectroscopy data analysis. Mach Learn Sci Technol 2020;1:15008.
- [68] Bravo-Sanchez M, Romero-Galarza A, Ramírez J, Gutiérrez-Alejandre A, Solís-Casados DA. Quantification of the sulfidation extent of Mo in CoMo HDS catalyst through XPS. Appl Surf Sci 2019;493:587–92. https://doi.org/10.1016/j.apsusc.2019.07.012.
- [69] Dalvi VH, Rossky PJ. Molecular origins of fluorocarbon hydrophobicity. Proc Natl Acad Sci U S A 2010;107:13603–7. https://doi.org/10.1073/pnas.0915169107.
- [70] Sheridan RP, Wang WM, Liaw A, Ma J, Gifford EM. Extreme gradient boosting as a method for quantitative structure-activity relationships. J Chem Inf Model 2016; 56:2353–60. https://doi.org/10.1021/acs.icim.6b00591.
- [71] Lei S. A feature selection method based on information gain and genetic algorithm. Int Conf Comput Sci Electron Eng 2012;2:355–8. https://doi.org/10.1109/ ICCSEE.2012.97.